Dynamics of simulated water under pressure

Francis W. Starr,[1,*] Francesco Sciortino,[2] and H. Eugene Stanley[1]
[1]*Center for Polymer Studies, Center for Computational Science, and Department of Physics, Boston University, Boston, Massachusetts 02215*
[2]*Dipartmento di Fisica e Istituto Nazionale per la Fisica della Materia, Universitá di Roma ''La Sapienza,'' Piazzale Aldo Moro 2, I-00185, Roma, Italy*
(Received 2 August 1999)

We present molecular dynamics simulations of the extended simple-point-charge model of water to probe the dynamic properties at temperatures from 350 K down to 190 K and pressures from 2.5 GPa (25 kbar) down to -300 MPa (-3 kbar). We compare our results with those obtained experimentally, both of which show a diffusivity maximum as a function of pressure. We find that our simulation results are consistent with the predictions of the mode-coupling theory for the dynamics of weakly supercooled liquids—strongly supporting the hypothesis that the apparent divergences of *dynamic* properties observed experimentally may be independent of a possible thermodynamic singularity at low temperature. The dramatic change in water's dynamic and structural properties as a function of pressure allows us to confirm the predictions of MCT over a much broader range of the von Schweidler exponent values than has been studied for simple atomic liquids. We also show how structural changes are reflected in the wave-vector dependence of dynamic properties of the liquid along a path of nearly constant diffusivity. For temperatures below the crossover temperature of MCT (where the predictions of MCT are expected to fail), we find tentative evidence for a crossover of the temperature dependence of the diffusivity from power-law to Arrhenius behavior, with an activation energy typical of a strong liquid. [S1063-651X(99)11712-4]

PACS number(s): 61.43.Fs, 64.70.Pf, 66.10.Cb

I. INTRODUCTION

The ''slow dynamics'' and glass transition of both simple and molecular liquids has been a topic of significant interest in recent years. The initial slowing down of liquids at temperatures down to $T_c \approx 1.2T_g$, where relaxation times approach 1 ns, has been well described by the mode-coupling theory (MCT) [1]. The MCT has been successfully applied to a wide variety of systems [2], including hard spheres [3], $Ni_{80}P_{20}$ [4], SiO_2 [5], and polymer melts [6]. However, there has not been an extensive test of the validity of the MCT predictions for a model system over a wide range of pressures and along different thermodynamic paths.

At low pressure, it was shown previously that the power-law behavior of dynamic properties in the extended simple-point-charge (SPC/E) model [7] can be explained using the MCT [8]. Furthermore, the possible relationship between the experimentally observed power-law behavior and the predictions of the MCT has been discussed [8–11]. The experimentally observed locus of apparent power-law singularities of dynamic and thermodynamic properties [Fig. 1] is of particular interest [12,13], and has catalyzed the development of three scenarios to explain the anomalous properties of water: (i) the existence of a spinodal bounding the stability of the liquid in the superheated, stretched, and supercooled states [12,15]; (ii) the existence of a liquid-liquid phase transition line separating two liquid phases differing in density [16–19]; (iii) a singularity-free scenario in which the thermodynamic anomalies are related to the presence of low-density and low-entropy structural heterogeneities [20]. The predictions of the MCT are of interest since the MCT might account for the apparent power-law behavior of dynamic properties on cooling, thereby removing the need for a thermodynamic explanation of the dynamic properties of water.

In this paper we focus on two related issues: (i) the possibility of using the MCT to explain the slow dynamics of water under pressure, and (ii) a test of the validity of the

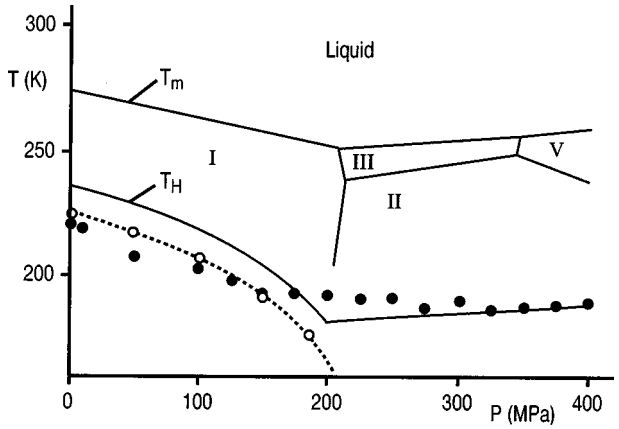

FIG. 1. Phase diagram of water. The extrapolated divergence of the isothermal compressibility (○) [14] and the extrapolated divergence of D (●) [9]. The different loci of these two singularity lines are consistent with the possibility that the two phenomena may arise from different explanations. Also shown are the melting line (T_m) and coexistence lines of several ice polymorphs and the experimental limit of supercooling (T_H).

*Present address: Polymers Division and Center for Theoretical and Computational Materials Science, National Institute of Standards and Technology, Gaithersburg, MD 20899. Electronic address: fstarr@nist.gov

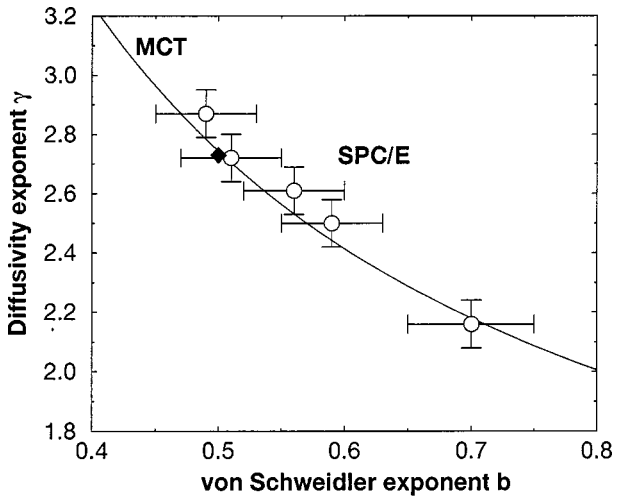

FIG. 2. The line shows the predicted relationship between b and γ from MCT. The symbols show the calculated values for the SPC/E model: (○) from this work, (filled ♦) from Ref. [8].

MCT predictions over a wide pressure range in a system with dramatic structural changes. We find that the MCT provides a good account of the slow dynamics of the SPC/E model for water at all pressures, with the structure evolving continuously from an open tetrahedral network to a densely packed fluid, similar to a Lennard-Jones-type liquid. By examining the wave-vector dependence of collective dynamics, we are able to discover how these structural changes are reflected in the dynamic behavior of the liquid. We are also able to test the validity of the relationship predicted by the MCT for the diffusivity exponent γ and the von Schweidler exponent b over a wide range of values γ and b [Fig. 2]. Our results support the predicted relationship of these exponents. A paper of a subset of the present results for the SPC/E potential has recently appeared [21]. The dynamic properties of the ST2 [22] and the TIP4P [23] potentials in a more limited pressure range, have also recently been discussed.

II. MODE-COUPLING THEORY

We will focus our discussion on the idealized form of the MCT, originally formulated to describe spherically symmetric potentials. Recent extensions have been made to account for the rotational motion present in nonspherical molecular systems [24], such as water. The idealized version of the MCT has been shown to provide a good account for the center-of-mass motion for the SPC/E model [8,25]. We provide only a brief account of the MCT predictions relevant to the results of this paper, and we refer the reader to extensive reviews for more information [1,2,26].

The MCT assumes that localization, or ''caging,'' of molecules due to the slow rearrangement of neighboring molecules is the source of the dramatic increase of relaxation times on cooling, leading to a strong coupling between single particle motion and the density fluctuations of the liquid. Indeed, according to the MCT, the *static* density fluctuations, measured by the structure factor $S(q)$, entirely determine the long-time dynamic behavior. The MCT accounts for the loss of correlation by the interaction of density mode fluctuations, ignoring other possible mechanisms for relaxation. The MCT predicts the asymptotic power-law divergence of correlation times, and power-law vanishing of the diffusion constant

$$D \sim D_0 (T/T_c - 1)^{\gamma} \tag{1}$$

at a critical temperature $T_c = T_c(P)$, where we refer to $\gamma = \gamma(P)$ as the diffusivity exponent. In real systems, ''freezing'' of the system dynamics is avoided at T_c, as relaxation mechanisms not accounted for by the MCT become significant. However, T_c can still be interpreted as a ''crossover temperature'' where the dynamics change from being dominated by density fluctuations to being controlled by ''activated'' processes. Some recent work has also demonstrated the significance of T_c as a crossover temperature where relaxation occurs primarily through basin hopping [27–30], in the energy landscape view of liquid dynamics [31,32].

MCT predicts that the Fourier transform of the density-density correlation function [33] or intermediate scattering function

$$F(q,t) \equiv \frac{1}{S(q)} \left\langle \sum_{j,k=1}^{N} e^{-i\mathbf{q}\cdot[\mathbf{r}_k(t) - \mathbf{r}_j(0)]} \right\rangle \tag{2}$$

decays via a two-step process. In the first relaxation step, $F(q,t)$ approaches a plateau value $F_{\text{plateau}}(q)$ which is described, to leading order in time, by a power law with exponent $a = a(P)$,

$$F(q,t) - F_{\text{plateau}}(q) \sim t^{-a}. \tag{3}$$

At larger times, $F(q,t)$ decreases from $F_{\text{plateau}}(q)$ and the MCT predicts the decay obeys the von Schweidler power law to leading order in time

$$F_{\text{plateau}}(q) - F(q,t) \sim t^{b}, \tag{4}$$

where $b = b(P)$ is known as the von Schweidler exponent. The region of validity of Eqs. (3) and (4) can be quite limited.

The slow relaxation of $F(q,t)$ has a characteristic relaxation time τ that is also predicted to have asymptotic power law dependence on temperature,

$$\tau \sim \tau_0 (T/T_c - 1)^{-\gamma} \tag{5}$$

with the same value of the exponent γ as for the diffusion constant. Hence, Eqs. (1) and (5) predict that the product $D\tau$ is not singular as $T \to T_c$, hence we take the product to be constant over the range that Eqs. (1) and (5) are valid (neglecting corrections to scaling).

The MCT predicts that the scaling exponents a, b, and γ are *not* independent; a and b are related by the exponent parameter λ using the relationship

$$\lambda = \frac{[\Gamma(1-a)]^2}{\Gamma(1-2a)} = \frac{[\Gamma(1-b)]^2}{\Gamma(1+2b)}, \tag{6}$$

where $\Gamma(x)$ is the gamma function. The MCT also relates γ to a and b via

$$\gamma = \frac{1}{2a} + \frac{1}{2b}. \tag{7}$$

TABLE I. Summary of the state points simulated with 216 molecules interacting via the SPC/E potential. For all state points, the uncertainty in the potential energy U is less than 0.05 kJ/mol. The uncertainty in the diffusion constant D is approximately ± 4, in the last digit shown. State points we equilibrated for a time t_{eq}, followed by ''data collection'' runs of duration t_{data}.

T (K)	ρ (g/cm^3)	U (kJ/mol)	P (MPa)	D (10^{-5} cm^2/s)	t_{eq} (ns)	t_{data} (ns)
190	1.00	−55.00	5±20	2.4×10^{-4}	60	200
200	1.00	−54.44	−1±18	1.5×10^{-3}	30	100
210	0.90	−53.45	−298±15	2.92×10^{-3}	8	100
	0.95	−53.84	−154±9	1.93×10^{-3}	25	100
	1.00	−53.70	−19±11	1.03×10^{-2}	35	100
	1.05	−53.43	80±12	2.27×10^{-2}	30	80
	1.10	−53.24	184±13	3.17×10^{-2}	30	80
	1.20	−53.13	461±14	3.04×10^{-2}	25	80
	1.30	−53.20	901±15	8.71×10^{-3}	25	100
	1.40	−52.98	1624±14	4.9×10^{-4}	30	100
220	0.95	−53.00	−150±6	1.68×10^{-2}	15	15
	1.00	−52.87	−21±10	3.89×10^{-2}	15	15
	1.05	−52.73	73±8	5.58×10^{-2}	15	15
	1.10	−52.59	187±8	8.47×10^{-2}	15	15
	1.15	−52.53	317±8	9.18×10^{-2}	2	15
	1.20	−52.48	480±9	8.01×10^{-2}	15	15
	1.25	−52.47	687±9	5.94×10^{-2}	3	15
	1.30	−52.49	951±12	2.63×10^{-2}	15	15
	1.40	−52.57	1670±15	1.69×10^{-3}	18	15
230	0.95	−52.14	−155±8	6.25×10^{-2}	4	5
	1.00	−52.06	−41±9	0.103	4	5
	1.05	−52.01	70±10	0.134	4	5
	1.10	−51.90	193±12	0.177	4	5
	1.20	−51.85	501±13	0.159	4	5
	1.30	−51.90	994±14	6.72×10^{-2}	4	5
	1.40	−51.82	1752±17	1.12×10^{-2}	4	5
240	0.95	−51.33	−153±8	0.141	7	5
	1.00	−51.35	−45±9	0.187	7	5
	1.05	−51.34	68±9	0.244	7	5
	1.10	−51.28	195±10	0.270	7	5
	1.20	−51.24	527±11	0.237	7	5
	1.30	−51.25	1035±4	0.135	7	5
	1.40	−51.24	1828±12	2.49×10^{-2}	12	5
260	0.95	−49.68	−148±9	0.504	5	3
	1.00	−49.87	−43±10	0.608	5	3
	1.05	−49.93	77±11	0.591	5	3
	1.10	−50.00	212±11	0.588	5	3
	1.20	−50.10	572±13	0.574	5	3
	1.30	−50.14	1127±14	0.354	5	3
	1.40	−49.97	1979±14	0.139	5	3
300	0.95	−46.80	−109±12	1.99	0.5	1
	1.00	−47.20	−13±13	2.00	0.5	1
	1.05	−47.49	112±14	1.83	0.5	1
	1.10	−47.65	264±14	1.82	0.5	1
	1.20	−47.95	678±16	1.53	0.5	1
	1.30	−48.06	1293±18	1.12	0.5	1
	1.40	−47.88	2222±19	0.495	0.5	1
350	0.90	−43.21	−105±16	6.11	0.5	40 ps
	1.00	−44.35	62±18	4.97	0.5	40 ps
	1.10	−45.15	358±20	3.81	0.5	40 ps
	1.20	−45.56	828±22	2.70	0.5	40 ps
	1.30	−45.76	1504±25	1.80	0.5	40 ps
	1.40	−45.50	2522±26	1.39	0.5	40 ps

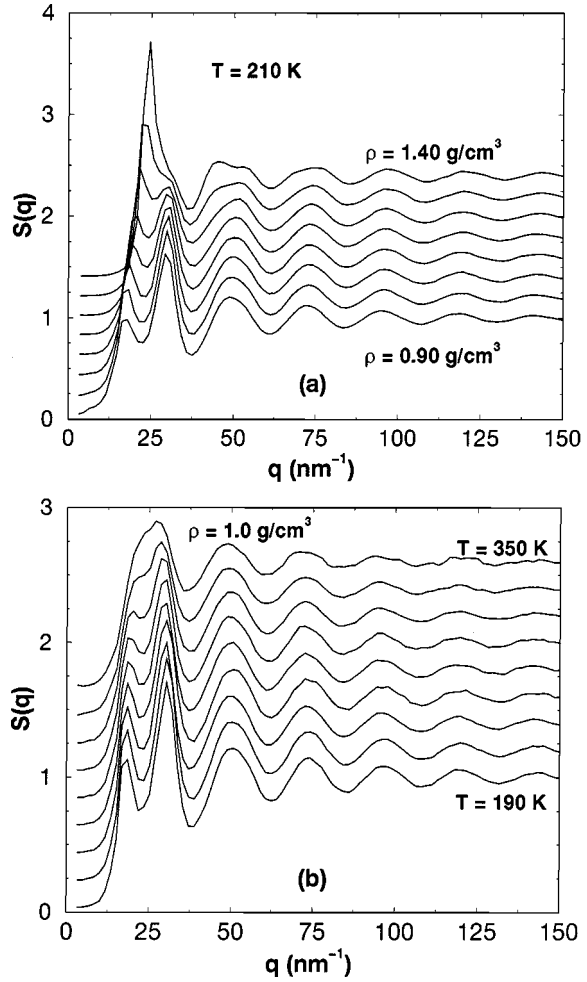

FIG. 3. The oxygen-oxygen structure factor $S(q)$: (a) Dependence on ρ for $T=210$ K. (b) T dependence along the $\rho=1.0$ g/cm^3 isochore. Notice that changing T has little effect, while changing ρ has a more pronounced effect. Each curve is offset by 0.2 for clarity.

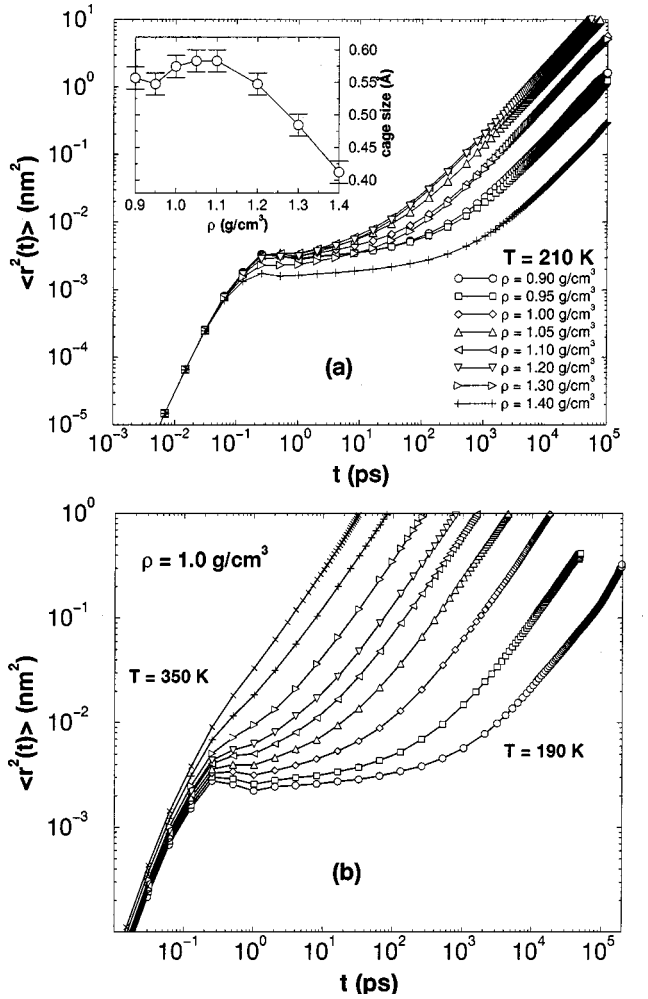

FIG. 4. Mean-squared displacement $\langle r^2(t)\rangle$ for (a) all densities at $T=210$ K and (b) all T along the $\rho=1.0$ g/cm^3 isochore. The inset of (a) shows the density dependence of the cage size.

Because of Eqs. (6) and (7), only one exponent value is needed to determine all others, so calculation of two exponents determines if the dynamics of a system are consistent with the predictions of the MCT. Furthermore, these exponents are expected to depend on the path along which T_c is approached.

After $F(q,t)$ departs from the plateau, $F(q,t)$ is well described by a Kohlrausch-Williams-Watts stretched exponential

$$F(q,t)=A(q)\exp\left[-\left(\frac{t}{\tau(q)}\right)^{\beta(q)}\right], \tag{8}$$

where $\tau(q)$ is the relevant relaxation time. Moreover, it has been shown that the exponent $\beta=\beta(q)$ is related to the von Schweidler exponent [34]

$$\lim_{q\to\infty}\beta(q)=b. \tag{9}$$

This relation facilitates evaluation of b, since the region of validity of Eq. (4) is difficult to identify in practice.

III. SIMULATIONS

We perform molecular-dynamics (MD) simulations of 216 water molecules interacting via the SPC/E pair potential [7]. The SPC/E model treats water as a rigid molecule consisting of three point charges located at the atomic centers of the oxygen and hydrogen, which have an OH distance of 1.0 Å and HOH angle of 109.47°, the tetrahedral angle. Each hydrogen has charge $q_H=0.4238e$, where e is the fundamental unit of charge, and the oxygen has charge $q_O=-2q_H$. In addition, the oxygen atoms of separate molecules interact via a Lennard-Jones potential with parameters $\sigma=3.166$ Å and $\epsilon=0.6502$ kJ/mol.

Our simulation results are summarized in Table I. For $T\leqslant 300$ K, we simulate two independent systems to improve statistics, as the long relaxation time makes time averaging more difficult. We equilibrate all simulated state points to constant T and ρ by monitoring the pressure and internal energy. We control the temperature using the Berendsen method of rescaling the velocities [35], while the reaction field technique with a cutoff of 0.79 nm [36] accounts for the long-range Coulombic interactions. The equations of motion evolve using the SHAKE algorithm [37] with a time step of 1 fs, except at $T=190$, where a time step of 2 fs is used due to the extremely slow motion of the molecules. Equilibration

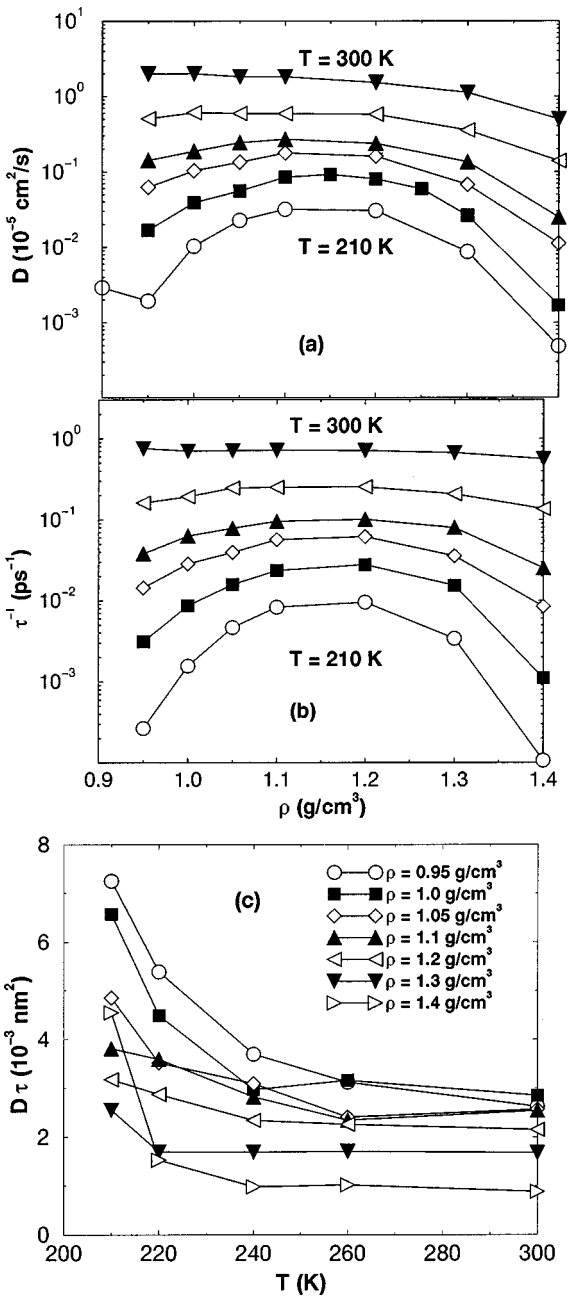

FIG. 5. (a) Diffusion constant D along isotherms for each density simulated. (b) Relaxation time τ of $F(q_0,t)$ along isotherms for each density simulated. (c) Test of the MCT prediction that $D\tau$ is constant along isochores.

times at high temperatures are relatively small. At low T, extremely long equilibration times are needed. The structural and thermodynamics properties may be obtained after relatively short equilibration times. However, dynamic properties show significant aging effects (i.e., dependence of measured properties on the chosen starting time) if great care is not taken in equilibration.

For production runs, it is desirable to make measurements in the isoenergetic/isochoric ensemble (NVE). However, a small energy drift is unavoidable for the long runs presented here, so we again employ the heat bath of Berendsen, using a relaxation time of 200 ps [8]. The large relaxation time prevents an energy drift but achieves results that are very close to those that would be found if it were possible to perform a simulation in the NVE ensemble.

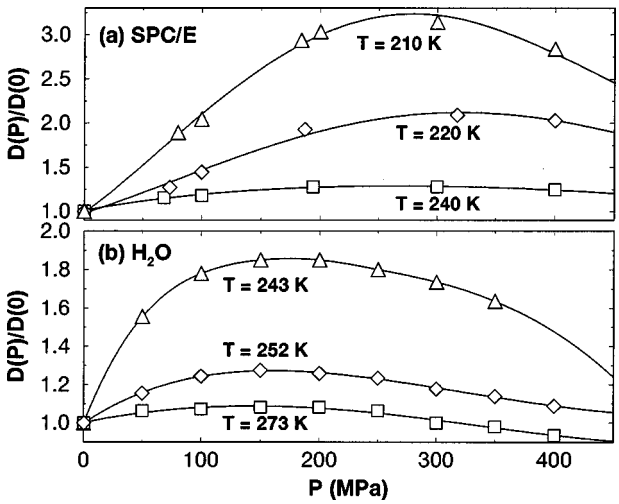

FIG. 6. D as a function of pressure for various temperatures from (a) our simulations and (b) NMR studies of water [9].

Since we perform long runs for many state points, we store the molecular trajectories $\{\mathbf{r}_i,\mathbf{p}_i\}$ at logarithmic intervals to avoid storage problems that linear sampling presents. Specifically, we sample configurations at times growing in powers of 2 up a maximum time $t_{\max}$. We begin a new sampling cycle each time $t_{\max}$ (relative to the cycle starting time) is reached. This sampling method allows for calculation of dynamic properties on time scales spanning eight orders of magnitude (from 1 fs to 100 ns) using a relatively small amount of disk space. Still, more than 2 GB of storage was required for the configurations at $T=210$ K. Our simulations have a speed of approximately 200 μs per update per molecule on a MIPS R10000 processor, representing a total calculation time of approximately 8.4 years of CPU time, including the systems of 1728 molecules discussed in the Appendix. For the larger systems, we utilize a parallelized version of our simulation code on eight processors to improve performance.

IV. STATIC STRUCTURE FACTOR

We first summarize the structural properties of our simulations in order to better understand the relationship between the changes in structure with the changes in dynamic behavior, which we will detail in Sec. VIII. Other studies have considered the structural and thermodynamic properties of SPC/E in a large region of the (P,T) plane [38–41], so the present discussion is brief.

The MCT theory requires as input the static density-density correlation functions. In the case of water, the structure of the system is very sensitive to the value of the external control parameter (P,T). Hence, for all state points simulated, we calculate the oxygen-oxygen partial structure factor [33]

$$S(q)\equiv\frac{1}{N}\left|\sum_{j=1}^{N} e^{-i\mathbf{q}\cdot\mathbf{r}_j}\right|^2. \tag{10}$$

Several studies have carefully calculated the structure of simulated water, and found surprisingly good agreement

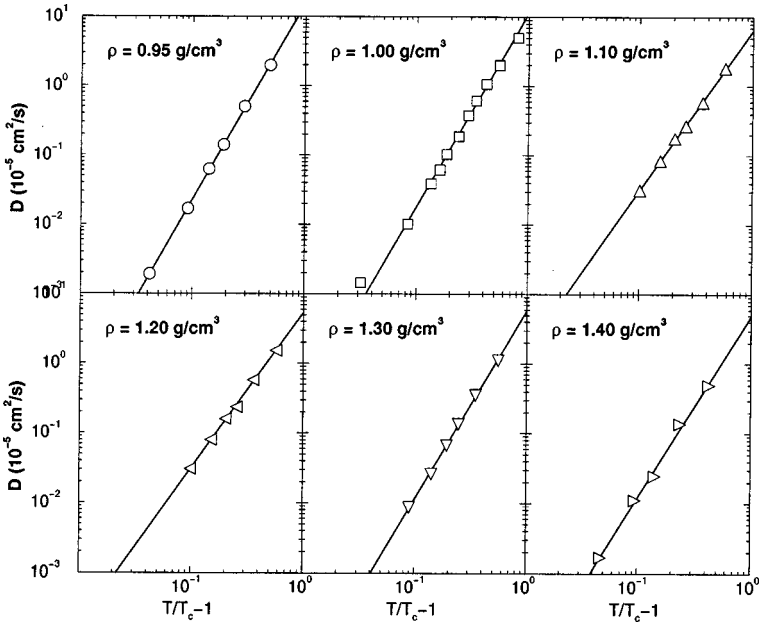

FIG. 7. Fit of each isochore to the power law $D \sim (T/T_c - 1)^{\gamma}$ predicted by MCT. We include the results of Ref. [43] along the $\rho = 1.0$ g/cm^3 isochore.

with experiments [16,41]. At $T = 210$ K, we show the structural changes from low to high density [Fig. 3(a)]. The structure at low density/pressure is similar to that observed for low-density amorphous (LDA) solid water, consisting of an open tetrahedral network. At high density/pressure, water is very similar to high-density amorphous (HDA) solid water, where core-repulsion dominates, similar to simple liquids under pressure.

We show the evolution of $S(q)$ as a function of T along the $\rho = 1.0$ g/cm^3 isochore in Fig. 3(b). We note that in the temperature range from 190 to 300 K, where the dynamics show the most dramatic change in behavior, $S(q)$ shows only small changes in the first two peaks. Also, the location of the first maximum q_0 in $S(q)$, the wave vector at which $F(q,t)$ typically shows the slowest relaxation, does not appear to change significantly. All other densities and temperatures show a relative smooth interpolation of Figs. 3(a) and 3(b).

V. MEAN-SQUARED DISPLACEMENT AND DIFFUSION

The mean-squared displacement $\langle r^2(t) \rangle \equiv \langle |\mathbf{r}(t) - \mathbf{r}(0)|^2 \rangle$ is shown in Fig. 4. All the curves show t^2

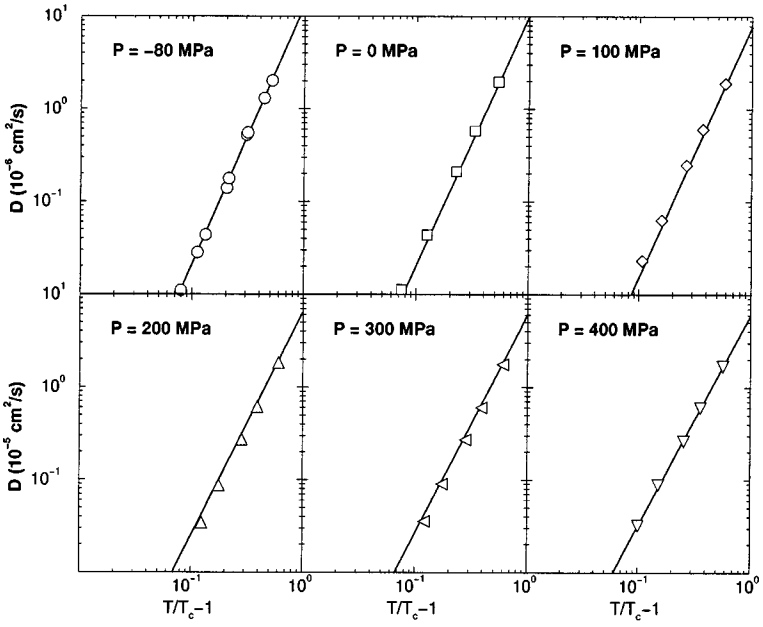

FIG. 8. Fit of the diffusion constant along each isobar to the power law $D \sim (T/T_c - 1)^{\gamma}$ predicted by MCT. We include the results of Ref. [8] along the -80 MPa isobar.

TABLE II. Fitting parameters to the power law predicted by the MCT, for $T \leqslant 300$ K. Note that the state points ($\rho = 1.00$ g/cm^3, $T = 200$ K, and $T = 190$ K) and ($\rho = 1.40$ g/cm^3, $T = 210$ K) are not included in the fit because they are very close to T_c, and so do not conform to the power law.

ρ (g/cm^3) or P (MPa)	D_0 (10^{-5} cm^2/s)	T_c (K)	γ
0.95	15.9	201.4	2.84
1.00	11.4	193.6	2.80
1.05	7.85	188.3	2.67
1.10	6.39	188.6	2.31
1.20	5.40	189.9	2.24
1.30	5.73	192.9	2.70
1.40	4.78	210.2	2.59
−80	13.3	197.9	2.79
0	10.2	193.9	2.62
100	7.72	187.8	2.61
200	6.51	188.8	2.50
300	6.08	188.8	2.42
400	5.91	190.7	2.25

dependence at small time, as expected in the ''ballistic'' regime.

For low T (e.g., $T = 210$ K [Fig. 4(a)]), $\langle r^2(t) \rangle$ shows relatively flat behavior over 3–4 decades in time. This is the ''cage'' region, in which a molecule is trapped by its neighbors and cannot diffuse, and is only vibrating within its cage. At low P, the cage consists of hydrogen-bonded neighbors in a tetrahedral configuration. This cage is relatively strong, compared to simple liquids, because of the H bonds. The size of the cage may be estimated by the value $\langle r^2(t) \rangle$ at the plateau, as shown in the inset of [Fig. 4(a)]. Surprisingly, the size of the cage is not monotonic with density, and has a maximum at $\rho \approx 1.1$ g/cm^3. We shall see that this corresponds roughly to the ρ at which D also has a maximum. We observe a small bump in $\langle r^2(t) \rangle$ at $t \approx 0.35$ ps, as observed in Ref. [8]. A system size study indicates that this may be attributed to finite size effects [42], and not to a Boson peak.

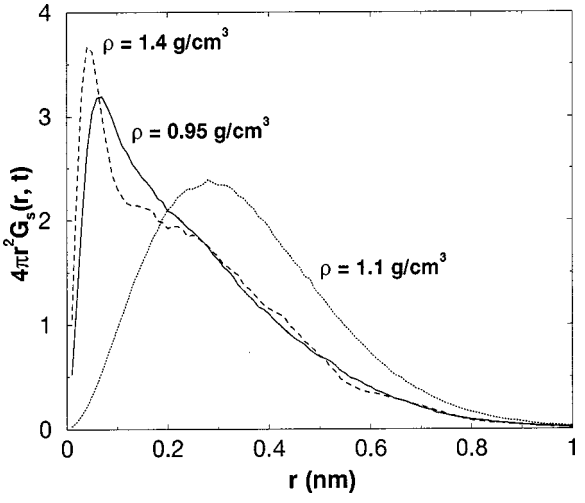

FIG. 9. The van Hove correlation function $G_s(r,t)$ for several densities at $T = 210$ K. For each curve, t is chosen such that $\langle r^2(t) \rangle \approx 0.1$ nm^2, well inside the diffusive regime [i.e., where $\langle r^2(t) \rangle$ is linear in t]. The presence of a pronounced shoulder in $G_s(r,t)$ for $\rho = 1.4$ g/cm^3 indicates that hopping phenomena are significant, and thus deviations from power-law dependence are expected.

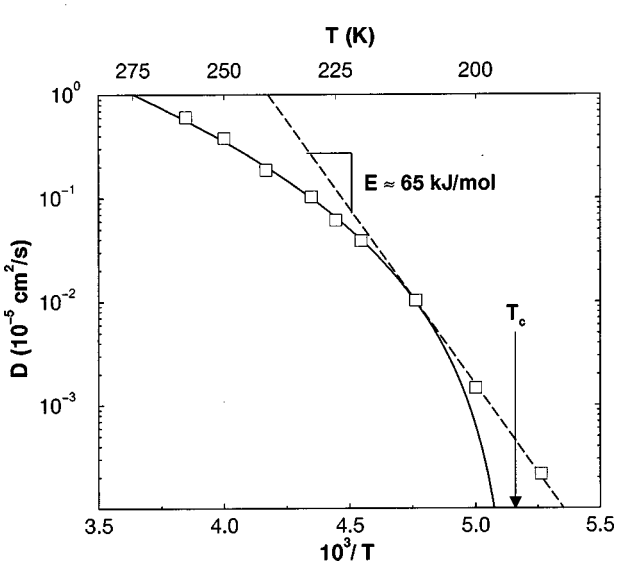

FIG. 10. Arrhenius plot of D shows that the power-law behavior (solid line) appears to make a smooth crossover to Arrhenius behavior (dashed line) for $T \lesssim T_c$ with activation energy $E \approx 65$ kJ/mol. This behavior may be related to a possible fragile-to-strong transition of the dynamic properties (see the discussion in text).

For long times, all the curves show linear t dependence, indicating that our simulations are in the diffusive regime. We extract the diffusion constant D using the asymptotic relation $\langle r^2(t) \rangle = 6Dt$. We plot the density dependence of D in Fig. 5 and find that the SPC/E potential, like water, shows an anomalous increase in D on increasing density. We also point out the feature that D shows a slight increase at very low density; namely, at $\rho = 0.90$ g/cm^3 and $T = 210$ K. This can be attributed to the fact that the liquid is extremely stretched at this density, causing an increase in the defects of the bond network, and thus increased diffusivity. We show D as a function of pressure along several isotherms to compare with experimental measurements [Fig. 6] [9]. The anomalous increase in D is qualitatively reproduced by our calculations for the SPC/E model, but the quantitative increase of D is significantly larger than that observed experimentally. This discrepancy may arise from the fact that the SPC/E potential is *understructured* relative to water [39], so applying pressure allows for more bond breaking and thus greater diffusivity than observed experimentally. We also find that the pressure where D begins to decrease with pressure — normal behavior for a liquid — is larger than that observed experimentally [9]. This comparison of D with experiment leads us to expect that while the qualitative dynamic features we observe in the SPC/E potential may aid in the understanding of the dynamics of water under pressure, they will likely not be quantitatively accurate.

We estimate D along the isobars $P = -80$, 0, 100, 200, 300, and 400 MPa from the isochoric data. We confirm that along the -80 MPa isobar, our estimates agree with the

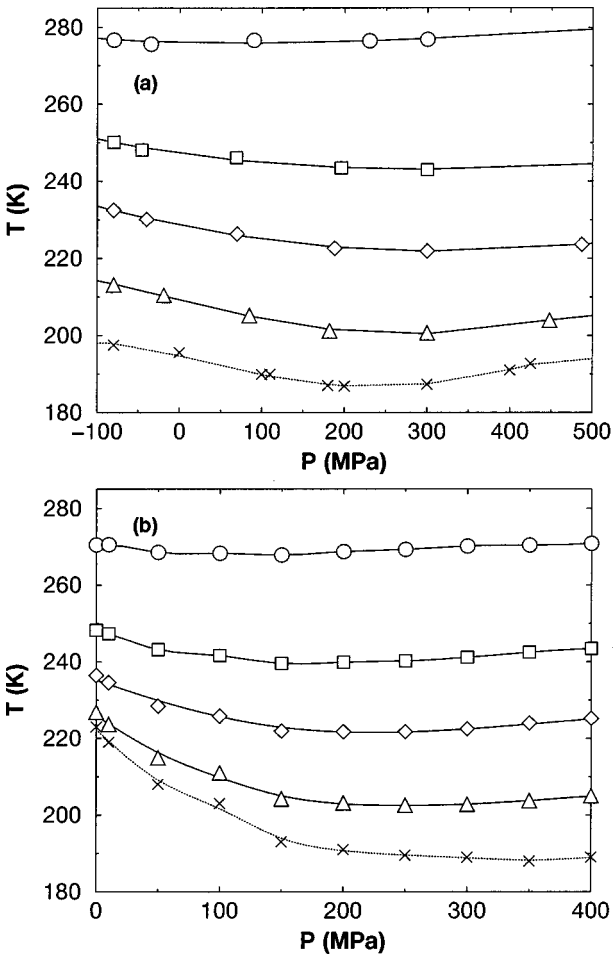

FIG. 11. (a) Isochrones of D from simulation. The lines may be identified at follows: $D=10^{-5}$ cm^2/s (○); $D=10^{-5.5}$ cm^2/s (□); $D=10^{-6}$ cm^2/s (◇); $D=10^{-7}$ cm^2/s (△). The diffusion is also fit to $D\sim(T-T_c)^{\gamma}$. The locus of T_c is indicated by (×). (b) Isochrones of D constructed from the experimental data in Ref. [9].

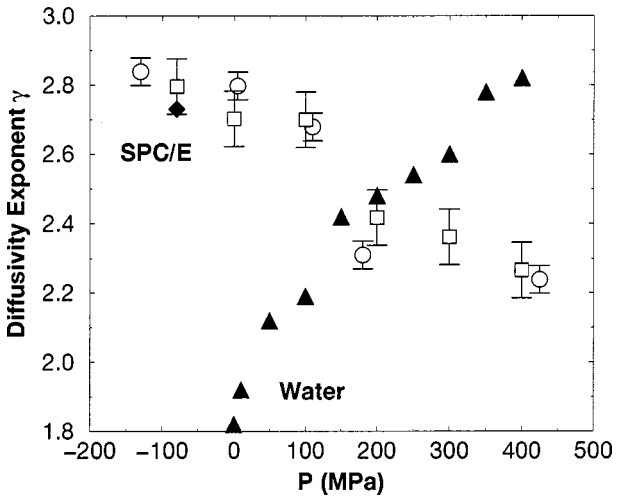

FIG. 12. Pressure dependence of the diffusivity exponent γ defined by $D\sim(T-T_c)^{\gamma}$. The symbols are as follows: (○) γ measured from simulation along isochores; (□) γ measured from simulation along isobaric paths, which are estimated from the isochoric data; (♦) γ measured along the -80 MPa isobar in Ref. [8]; (▲) experimental measurements of γ in water from Ref. [9]. It is clear that the SPC/E potential fails to reproduce the qualitative behavior of γ under pressure in liquid water.

-80 MPa calculations of Ref. [8], which employs the same truncation of the potential used here (see Sec. III). Along the 0 MPa isobar, our estimates of D are smaller than those calculated for SPC/E in Ref. [38], perhaps because Ref. [38] chooses a different truncation of the electrostatic terms—highlighting the extreme sensitivity of the dynamics to changes in the potential.

We fit D by the power law of Eq. (1) along both isochores and the estimated isobars for $T\leqslant 300$ K [Figs. 7 and 8]. The values of the two fit parameters T_c and γ are given in Table II [44]. We also include the data from Ref. [43] along the $\rho=1.0$ g/cm^3 isochore and from Ref. [8] along the $P=-80$ MPa isobar to improve the quality of the fits. At $\rho=1.40$ g/cm^3, we exclude $T=210$ K when fitting D and obtain $T_c=209.3$, since we expect the power law of Eq. (1) to fail for $T\lesssim T_c+5$ K, because activated processes—such as ''hopping'' not accounted for in the idealized MCT—become significant and aid diffusion. To demonstrate the presence of hopping at $\rho=1.40$ and $T=210$ K, we plot the ''self'' part of the van Hove correlation function $G_s(r,t)$, which measures the distribution of particle displacements r at time t, for several densities at $T=210$ K [Fig. 9]. For these densities where a power law adequately describes D, there is a single peak. At $\rho=1.40$ g/cm^3, we see a ''shoulder'' in $G_s(r,t)$ at $r\approx 0.2$ nm in addition to a well-defined peak at $r\approx 0.05$ nm, indicating that particle hopping is significant.

Along the $\rho=1.00$ g/cm^3 we have simulated to significantly lower T, allowing us to study the temperature dependence of D for $T\lesssim T_c$. Figure 10 shows that the lowest temperatures are consistent with the Arrhenius form

$$D=D_{\infty}\exp(-E/k_BT). \tag{11}$$

Arrhenius temperature dependence of D is not surprising in this region, since for $T<T_c$ it is expected that the energy barriers the system must overcome to rearrange exceed the thermal energy [27]. Hence the motion of the system is dominated by activated jumps over the energy barriers, as described by Goldstein [31]. We obtain an activation energy of $E\approx 65$ kJ/mol and extrapolate a glass transition temperature $T_g\approx 125$ K [45], surprisingly close to the experimental value of 136 K [46]. The extrapolated value of T_g is similar to that estimated in Ref. [43] which studied hydrogen bond dynamics. Moreover, our results are consistent with a crossover from ''fragile'' behavior (the behavior described by MCT) for $T\gtrsim T_c$, to ''strong'' behavior (Arrhenius behavior with $E\approx k_BT_g/25\approx 40$ kJ/mol for our estimate of T_g) for $T\lesssim T_c$. The possibility of a ''fragile-to-strong'' crossover in water has been suggested based on experimental findings [47], while other recent experiments suggest no such transition exists [48]. Lower temperatures are required to conclusively test this possibility in the SPC/E model.

VI. ISOCHRONES OF D AND THE LOCUS OF $T_C(P)$

To construct isochrones of D (lines of constant D), we first estimate $T(D)$ at values of $D=10^{-5}$ cm^2/s, $10^{-5.5}$ cm^2/s, 10^{-6} cm^2/s, and 10^{-7} cm^2/s, using the fits of Figs. 7 and 8. Along the isobaric paths, we know already P

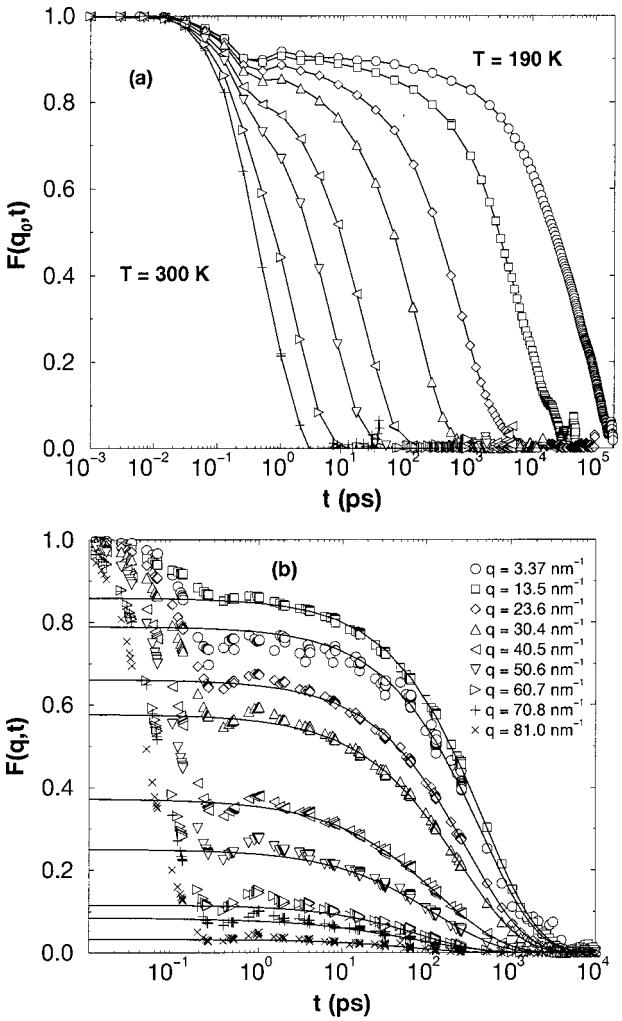

FIG. 13. The intermediate scattering function $F(q,t)$ (a) for $190 \leqslant T \leqslant 300$ K along the $\rho = 1.0$ g/cm^3 isochore and (b) for many q values at $T = 210$ K and $\rho = 1.00$ g/cm^3. The solid line shows the fit to Eq. (8) for $t \geqslant 2$ ps.

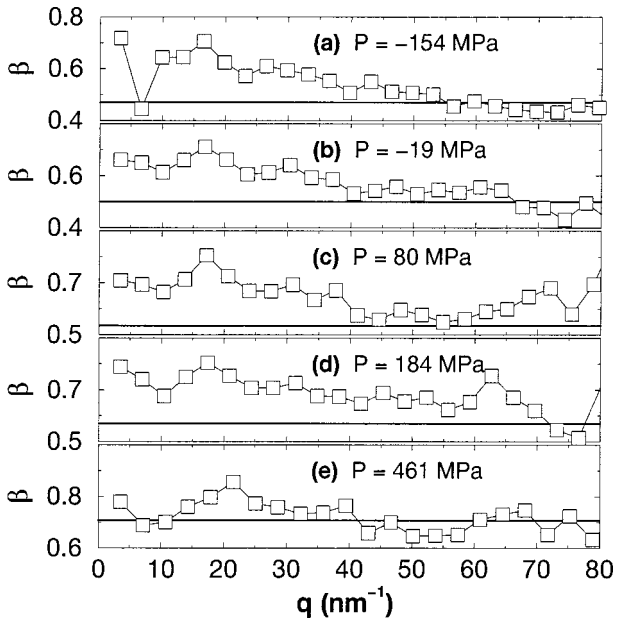

FIG. 14. Fit of the stretched exponential of Eq. (8) for $t \geqslant 2$ ps at $T = 210$ K to $F(q,t)$ to obtain: (b). The horizontal line indicates the value predicted by MCT for b using γ values extrapolated from Fig. 12. For $P \gtrsim 80$ MPa, the relaxation of $F(q,t)$ for $q \gtrsim 60$ nm^{-1} comes almost entirely from the first decay region, so the β values obtained are not reliable in this range.

for these points, and along isochores we may estimate the value of P using the results presented in Table I. We plot the isochrones in Fig. 11.

We also show the loci of $T_c(P)$ in Fig. 11(a), obtained from the fits in the previous section. We know P at T_c along the isobaric paths, and we estimate the P at T_c along isochores by extrapolating P in Table I to T_c.

Using the experimental diffusion data of Ref. [9], we also construct the behavior of the experimental isochrones following the same technique [Fig. 11(b)]. The shape of the locus of $T_c(P)$ compares well with that observed experimentally [9] (Fig. 11). Therefore, an explanation of the SPC/E dynamics using the MCT would support using the MCT framework as an interpretation of the experimentally found locus of $T_c(P)$. We find, however, that γ decreases with P for the SPC/E model, while γ increases with P [Fig. 12]. This disagreement underscores the need to improve the dynamic properties of water models, most of which already provide an adequate account of static properties [49].

VII. INTERMEDIATE SCATTERING FUNCTION

We plot the intermediate scattering function $F(q_0,t)$ in Fig. 13(a) for all T along the $\rho = 1.00$ g/cm^3 isochore, where $q_0 = 18.55$ nm^{-1}, the approximate value of the first peak of $S(q)$ where the relaxation of $F(q,t)$ is slowest. We define the relaxation time τ by $F(t=\tau) = e^{-1}$. We show τ along isotherms in Fig. 5(b), from which it is obvious that τ has very similar behavior to D^{-1}. Indeed, the MCT predicts that the product $D\tau$ is constant along isochores, which we test in Fig. 5(c). We find that $D\tau$ increases slightly on cooling, but remains relatively constant along each isochore. The weak residual T dependence in $D\tau$ should be subjected to a deeper scrutiny to find out if it is related to a q-vector-dependent correction to scaling (since D is a $q = 0$ quantity) or to the progressive breakdown of the validity of the ideal MCT on approaching T_c.

The study of the time dependence of $F(q_0,t)$ allows us to test the predicted relation between the exponents b and γ [see Eqs. (6) and (7)]. Since the value of b is completely determined by the value of γ [26], calculation of these exponents for SPC/E determines if MCT is consistent with our results. The range of validity of the von Schweidler power law [Eq. (4)] is strongly q dependent [51], making unambiguous calculation of b difficult.

Fortunately, according to the MCT [34], at large q vectors, the stretching exponent $\beta(q)$, which characterizes the the long-time behavior of $F(q,t)$ [see Eq. (8)], is controlled by the same exponent b at large q. Fits of $F(q,t)$ according to Eq. (8) are shown for many q values at $T = 210$ K and $\rho = 1.00$ g/cm^3. The same fit quality is observed for all other low T state points. The q dependence of $\beta(q)$ for $\rho \leqslant 1.30$ g/cm^3 and $T = 210$ K is shown in Fig. 14 [50] for $F(q,t)$. In addition, we show the expected value of b according to MCT, using the values of γ extrapolated from Fig. 12. The large-q limit of β appears to approach the value predicted by the MCT. Hence we conclude that the dynamic

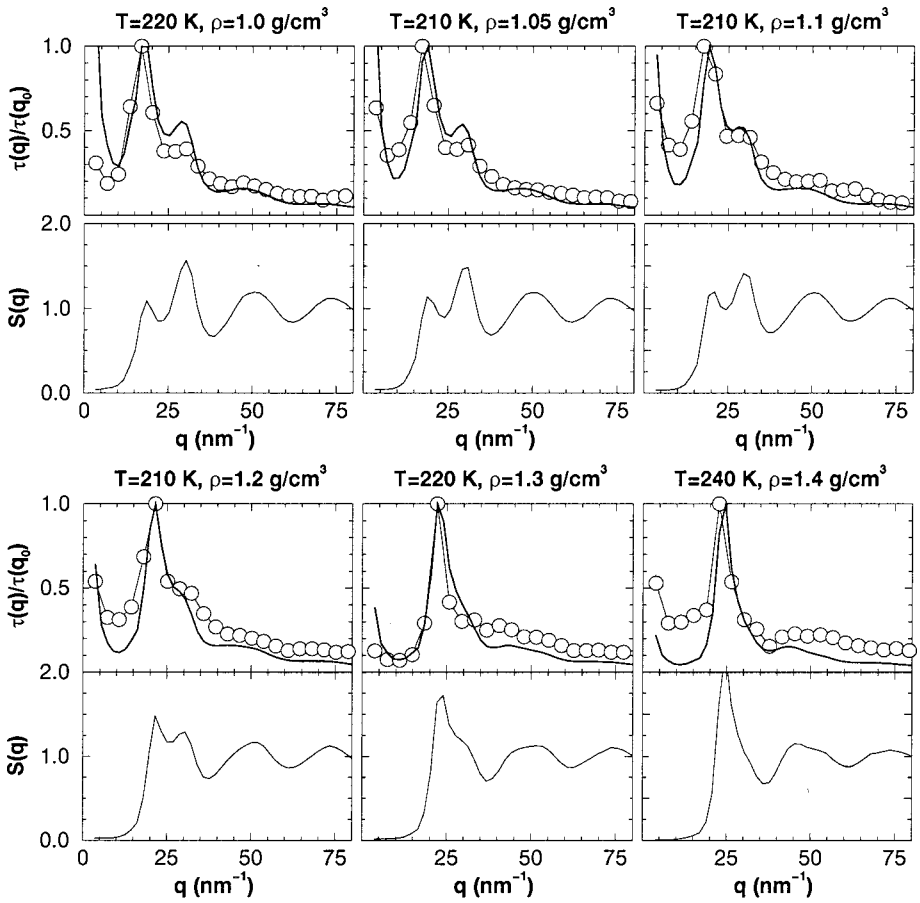

FIG. 15. Fitting parameter $\tau(q)$ of Eq. (8) in relation to $S(q)$ along approximate isochrones. The heavy line indicates the prediction $\tau \sim S(q)/q^2$.

behavior of the SPC/E potential in the pressure range we study is consistent with slowing down as described by MCT [Fig. 2]. We also checked that the values of b calculated from Eq. (9) are consistent with the von Schweidler power law Eq. (4), but that corrections to scaling in t^{2b} are relevant at several q vectors, as discussed in Ref. [8].

VIII. RELATIONSHIP OF STRUCTURE TO DYNAMICS

The results shown in Fig. 14, and the observed power-law dependence of diffusivity, suggest that MCT is able to predict the dynamical behavior of SPC/E water in a wide range of P and T. As discussed above, the structure of the liquid changes significantly under increased pressure. To highlight the effect of structural changes on dynamic properties, we consider an approximately isochronic path—along which D remains nearly constant—such that the changes in dynamic properties we observe on increasing P are confined to their q-vector dependence. We select five state points with $D=(0.030\pm0.009)\times10^{-5}$ cm^2/s: (i) $T=220$ K, $\rho=1.00$ g/cm^3, (ii) $T=210$ K, $\rho=1.05$ g/cm^3, (iii) $T=210$ K, $\rho=1.10$ g/cm^3, (i) $T=210$ K, $\rho=1.20$ g/cm^3, (iv) $T=220$ K, $\rho=1.30$ g/cm^3, and (v) $T=240$ K, $\rho=1.40$ g/cm^3. We show in Fig. 15 the q dependence of the α-relaxation time $\tau(q)$ extracted from the fit of $F(q,t)$ to the stretched exponential of Eq. (8). For all state points, the q dependence of τ follows the q dependence of $S(q)$, as commonly observed in supercooled liquids and in solutions of the full q-vector-dependent mode-coupling equations. We also note that $\tau(q)$ is well described by the relation

$$\tau(q) \propto S(q)/q^2 \tag{12}$$

(the deGennes narrowing relation [52]), as shown in the same figure. The MCT prediction for the q dependence of τ is often very close to the relation (12).

IX. DISCUSSION

We have presented extensive simulations that provide further evidence for interpreting the dynamics of the SPC/E potential in the framework of of MCT. Our calculations also provide a necessary test of the relation predicted between the diffusivity exponent γ and the von Schweidler exponent b for a wide range of values γ and b. Our results support interpretation of the experimental locus $T_c(P)$ as the locus of the MCT transitions.

We found that on increasing pressure, the values of the exponents become closer to those for hard-sphere ($\gamma=2.58$ and $b=0.545$) and Lennard-Jones ($\gamma=2.37$ and $b=0.617$) systems [53], thereby confirming that the hydrogen-bond network is destroyed under pressure and that the water dynamics become closer to that of normal liquids, where core repulsion dominates. A significant result of our analysis is the demonstration that the MCT is able to rationalize the dynamic behavior of the SPC/E model of water at all pressures. In doing so, MCT encompasses both the behavior at low pressures, where the mobility is essentially controlled by

TABLE III. Summary of the state points simulated with 1728 molecules to check for finite-size effects. For both state points, the uncertainty in the potential energy U is less the 0.04 kJ/mol.

T	ρ (g/cm^3)	U (kJ/mol)	P (MPa)	D (10^{-6} cm^2/s)	t_{eq} (ns)	t_{data} (ns)
190	1.00	-55.12	6 ± 8		60	40
200	1.00	-54.41	-4 ± 7	0.0020 ± 0.0007	30	35

the presence of strong energetic cages of hydrogen bonds, and at high pressures, where the dynamics are dominated by excluded volume effects. We also showed how these structural changes are reflected in the q dependence of $F(q,t)$.

Our results underscore the need to improve the dynamic properties of potentials for realistic simulations of water and other other materials. Of the many potentials available for studying water, only the SPC/E potential is known to display the power-law dependence of dynamic properties, but even SPC/E fails to reproduce the power law quantitatively. A recent study of the ST2 potential [54] found that the T dependence of D is consistent with an Arrhenius T dependence for $T\gtrsim300$ K, crossing over to another region of Arrhenius behavior for $T\lesssim275$ K [22], in contrast to the non-Arrhenius behavior observed in real water and to our interpretation based on the MCT for $T\geqslant T_c$. The presence of a low-T Arrhenius regime in the ST2 potential might be due to activated processes, which are expected to dominate the dynamics of fragile liquids below T_c, as we observed for the SPC/E potential. Hence the ST2 potential may provide an excellent opportunity to study these activated processes on a smaller time scale than is typically observed for most fragile liquids.

Finally, we stress that a full comparison between theory and simulation data requires a complete solution of the recently proposed molecular-MCT (the extension of MCT to molecules of arbitrary shape) [24]. A detailed solution of the complicated molecular-MCT equations in such large region of T and P values would require computational effort beyond the present possibilities, but a detailed comparison between molecular-MCT and MD data for one selected isobar is underway [55].

ACKNOWLEDGMENTS

We thank C. A. Angell, A. Geiger, E. La Nave, A. Rinaldi, S. Sastry, A. Scala, and R. J. Speedy for enlightening discussions and comments on the manuscript. We especially thank S. Harrington for his contributions to the early stages of this work. We thank the Boston University Center for Computational Science for access to the 192 processor SGI/Cray Origin supercomputer. F.S. is supported in part by MUSRT (PRIN 98). The Center for Polymer Studies is supported by the NSF Grant No. CH9728854.

APPENDIX: FINITE-SIZE EFFECTS

Some recent work [28,29] indicates that significant finite-size effects can affect results at temperatures close to the MCT T_c. Most of our systems are farther than 5% from T_c (i.e., $T/T_c-1\lesssim0.05$) so that the relatively small size of our system should not affect our results. We simulated two independent systems of 1728 molecules at both $T=200$ and 190 K and $\rho=1.00$ g/cm^3 to check if significant finite size effects appear at low T. The results are shown in Table III. We observe no significant deviations from the system of 216 molecules at $T=200$ K. Hence we believe that no strong finite-size effects are present in the 216 molecule system for $T\geqslant200$ K.

However, at $T=190$ K, the potential energy of the 1728 molecule system appears to be significantly smaller than that of the smaller system. We lack adequate computer resources to make a reliable estimate the diffusivity in the larger system, but simulations are continuing in order to check the possible finite-size effects at this temperature. From a physical standpoint, the value of D calculated at 190 K in the small system leads to the Arrhenius behavior with $E\approx65$ kJ/mol. This value is appealing, since it corresponds closely the value of E obtained for an Arrhenius fit of D in ice Ih [56]. In other words, at these low temperatures, the liquid is locally very similar to the crystal, and hence any reordering should require a similar activation energy. Of course, this does not preclude that the finite size of the system may change D.

The most likely effect on D due to finite size, if any, would be to increase D, since at very low T, the finite size would likely prevent the system from sampling some regions of phase space that help to reorder the system, and thus diffuse. If D could still be fit by an Arrhenius law, then the value of E would be smaller, and closer to that expected for a strong liquid with $T_g=125$ K (see the end of Sec. V). Beyond such an effect, we do not expect any significant change in the conclusions presented here.

[1] W. Götze and L. Sjögren, Rep. Prog. Phys. **55**, 241 (1992).
[2] See, e.g., special issue of Transport Theory Stat. Phys. **24** (1995), devoted to experimental and computational tests of MCT.
[3] J. L. Barrat, W. Götze, and A. Latz, J. Phys.: Condens. Matter **M1**, 7163 (1989); P. N. Pusey and W. van Megen, Phys. Scr. **T45**, 261 (1992).
[4] W. Kob and H. C. Andersen, Phys. Rev. Lett. **73**, 1376 (1994); Phys. Rev. E **51**, 4626 (1995); **52**, 4134 (1995).
[5] J. Horbach, W. Kob, and K. Binder, Philos. Mag. B **77**, 297 (1998); J. Horbach and W. Kob, Phys. Rev. B **60**, 3169 (1999).
[6] C. Bennemann, W. Paul, K. Binder, and B. Dünweg, Phys. Rev. E **57**, 843 (1998); C. Bennemann, J. Baschnagel, and W. Paul, Eur. Phys. J. B **10**, 323 (1999).
[7] H. J. C. Berendsen, J. R. Grigera, and T. P. Stroatsma, J. Phys. Chem. **91**, 6269 (1987).
[8] P. Gallo, F. Sciortino, P. Tartaglia, and S.-H. Chen, Phys. Rev. Lett. **76**, 2730 (1996); F. Sciortino, P. Gallo, P. Tartaglia, and S.-H. Chen, Phys. Rev. E **54**, 6331 (1996); S.-H. Chen, P. Gallo, F. Sciortino, and P. Tartaglia, *ibid.* **56**, 4231 (1997); F. Sciortino, L. Fabbian, S.-H. Chen, and P. Tartaglia, *ibid.* **56**, 5397 (1997).

[9] F. X. Prielmeier, E. W. Lang, R. J. Speedy, and H.-D. Lüdemann, Phys. Rev. Lett. **59**, 1128 (1987); Ber. Bunsenges. Phys. Chem. **92**, 1111 (1988).
[10] A. P. Sokolov, J. Hurst, and D. Quitmann, Phys. Rev. B **51**, 12 865 (1995).
[11] H. Weingärtner, R. Haselmeier, and M. Holz, J. Phys. Chem. **100**, 1303 (1996).
[12] C. A. Angell, in *Water: A Comprehensive Treatise*, edited by F. Franks (Plenum, New York, 1981).
[13] P. G. Debenedetti, *Metastable Liquids* (Princeton University Press, Princeton, 1996).
[14] H. Kanno and C. A. Angell, J. Chem. Phys. **70**, 4008 (1979).
[15] R. J. Speedy and C. A. Angell, J. Chem. Phys. **65**, 851 (1976); R. J. Speedy, *ibid.* **86**, 892 (1982).
[16] P. H. Poole, F. Sciortino, U. Essmann, and H. E. Stanley, Nature (London) **360**, 324 (1992); Phys. Rev. E **48**, 3799 (1993); F. Sciortino, P. H. Poole, U. Essmann, and H. E. Stanley, *ibid.* **55**, 727 (1997); S. Harrington, R. Zhang, P. H. Poole, F. Sciortino, and H. E. Stanley, Phys. Rev. Lett. **78**, 2409 (1997).
[17] O. Mishima, J. Chem. Phys. **100**, 5910 (1994).
[18] C. J. Roberts, A. Z. Panagiotopoulos, and P. G. Debenedetti, Phys. Rev. Lett. **97**, 4386 (1996); C. J. Roberts and P. G. Debenedetti, J. Chem. Phys. **105**, 658 (1996).
[19] M.-C. Bellissent-Funel, Europhys. Lett. **42**, 161 (1998); O. Mishima and H. E. Stanley, Nature (London) **392**, 192 (1998); **396**, 329 (1998).
[20] S. Sastry, F. Sciortino, P. G. Debenedetti, and H. E. Stanley, Phys. Rev. E **53**, 6144 (1996); L. P. N. Rebelo, P. G. Debenedetti, and S. Sastry, J. Chem. Phys. **109**, 626 (1998); H. E. Stanley and J. Teixeira, *ibid.* **73**, 3404 (1980); E. LaNave, S. Sastry, F. Sciortino, and P. Tartagglia, Phys. Rev. E **59**, 6348 (1999).
[21] F. W. Starr, S. Harrington, F. Sciortino, and H. E. Stanley, Phys. Rev. Lett. **82**, 3629 (1999).
[22] D. Paschek and A. Geiger, J. Phys. Chem. B **103**, 4139 (1999).
[23] H. Tanaka, J. Chem. Phys. **105**, 5099 (1996).
[24] R. Schilling and T. Scheidsteger, Phys. Rev. E **56**, 2932 (1997); T. Franosch, M. Fuchs, W. Götze, M. R. Mayr, and A. P. Singh, *ibid.* **56**, 5659 (1997); L. Fabbian, F. Sciortino, F. Thiery, and P. Tartaglia, Phys. Rev. E **57**, 1485 (1998); L. Fabbian, A. Latz, R. Schilling, F. Sciortino, P. Tartaglia, and C. Theis, e-print cond-mat/9812363.
[25] In this work we study the motion of oxygen atoms, and not the center of mass motion. However, for the SPC/E model, the center of mass is offset from the oxygen along the H-O-H bisector by only 0.06 Å so the difference is negligible.
[26] W. Götze, in *Liquids, Freezing, and Glass Transition*, edited by J. P. Hansen, D. Levesque, and J. Zinn-Justin, Proceedings of les Houches (North-Holland, Amsterdam, 1991).
[27] F. Sciortino and P. Tartaglia, Phys. Rev. Lett. **78**, 2385 (1998).
[28] W. Kob, C. Donati, S. J. Plimpton, and S. C. Glotzer, Phys. Rev. Lett. **79**, 2827 (1997); C. Donati, J. F. Douglas, W. Kob, S. J. Plimpton, P. H. Poole, and S. C. Glotzer, *ibid.* **80**, 2338 (1998).
[29] S. Sastry, P. G. Debenedetti, and F. H. Stillinger, Nature (London) **393**, 554 (1998).
[30] T. B. Schrøder, S. Sastry, J. C. Dyre, and S. C. Glotzer, e-print cond-mat/9901271.
[31] M. Goldstein, J. Chem. Phys. **51**, 3728 (1969).
[32] C. A. Angell, Science **267**, 1924 (1995); F. H. Stillinger, *ibid.* **267**, 1935 (1995).
[33] J. P. Hansen and I. R. McDonald, *Theory of Simple Liquids* (Academic Press, London, 1986).
[34] M. Fuchs, J. Non-Cryst. Solids **172**, 241 (1994).
[35] H. J. C. Berendsen *et al.*, J. Chem. Phys. **81**, 3684 (1984).
[36] O. Steinhauser, Mol. Phys. **45**, 335 (1982).
[37] J.-P. Ryckaert, G. Ciccotti, and H. J. C. Berendsen, J. Comput. Phys. **23**, 327 (1977).
[38] L. A. Baez and P. Clancy, J. Chem. Phys. **101**, 9837 (1994).
[39] S. Harrington, P. H. Poole, F. Sciortino, and H. E. Stanley, J. Chem. Phys. **107**, 7443 (1997).
[40] K. Bagchi, S. Balasubramanian, and M. Klein, J. Chem. Phys. **107**, 8561 (1997).
[41] F. W. Starr, M.-C. Bellissent-Funel, and H. E. Stanley, Phys. Rev. E **60**, 1084 (1999).
[42] F. Sciortino and F. W. Starr (unpublished).
[43] F. W. Starr, J. K. Nielsen, and H. E. Stanley, Phys. Rev. Lett. **82**, 2294 (1999).
[44] We note that the data for D may also be fit by the Vogel-Fulcher-Tammann form with an ''ideal'' glass-transition temperature T_0. A detailed study of the ideal glass transition in terms of the ''configurational'' entropy of the liquid is currently underway [A. Scala, F. W. Starr, E. La Nave, F. Sciortino, and H. E. Stanley, e-print cond-mat 9908301.
[45] We estimate T_g by extrapolating Eq. (11) to the temperature where D reaches 10^{-18} cm^2/s, a typical value of D at the glass transition.
[46] C. A. Angell and E. J. Sare, J. Chem. Phys. **52**, 1058 (1970).
[47] C. A. Angell, J. Phys. Chem. **97**, 6339 (1993); K. Ito, C. T. Moynihan, and C. A. Angell, Nature (London) **398**, 492 (1999); F. W. Starr, C. A. Angell, R. J. Speedy, and H. E. Stanley, e-print cond-mat/9903451.
[48] R. S. Smith and B. D. Kay, Nature (London) **398**, 288 (1999).
[49] SiO_2, another network-forming fluid, confirms the sensitivity of the dynamics on the model potential [M. Hemmati and C. A. Angell, in *Physics Meet Geology*, edited by H. Aoki and R. Hemley (Cambridge University Press, Cambridge, 1998)].
[50] We do not show the behavior of $\beta(q)$ for $\rho=1.40$ g/cm^3 and $T=210$ K since the MCT predictions are not expected to be valid for this state point, as discussed in Sec. V.
[51] T. Franosch, M. Fuchs, W. Götze, M. R. Mayr, and A. P. Singh, Phys. Rev. E **55**, 7153 (1997).
[52] P. G. deGennes, Physica (Utrecht) **25**, 825 (1959).
[53] For hard spheres, see J. L. Barrat, W. Götze, and A. Latz, J. Phys.: Condens. Matter **M1**, 7163 (1989); for Lennard-Jones, see U. Bengtzelius, Phys. Rev. A **34**, 5059 (1986).
[54] F. H. Stillinger and A. Rahman, J. Chem. Phys. **60**, 1545 (1974).
[55] L. Fabbian, A. Latz, R. Schilling, F. Sciortino, P. Tartaglia, and C. Theis, Phys. Rev. E (to be published).
[56] L. Onsager and L. K. Runnels, J. Chem. Phys. **50**, 1089 (1969); K. Goto, T. Hondoh, and A. Higashi, Jpn. J. Appl. Phys., Part 1 **25**, 351 (1986).